# Localized Reduced Basis Approximation of a Nonlinear Finite Volume Battery Model with Resolved Electrode Geometry*

Mario Ohlberger[†]        Stephan Rave[*]

June 15, 2016

**Abstract**

In this contribution we present first results towards localized model order reduction for spatially resolved, three-dimensional lithium-ion battery models. We introduce a localized reduced basis scheme based on non-conforming local approximation spaces stemming from a finite volume discretization of the analytical model and localized empirical operator interpolation for the approximation of the model's nonlinearities. Numerical examples are provided indicating the feasibility of our approach.

## 1    Introduction

Over the recent years, three dimensional lithium (Li) ion battery models that fully resolve the microscopic geometry of the battery electrodes have become a subject of active research in electrochemistry [10]. These models are also studied in the collaborative research project MULTIBAT, where the influence of the microscopic electrode geometry plays in important role in understanding the degradation process of Li-plating [9].

Due to the strongly nonlinear character of these models and the large number of degrees of freedom of their discretization, numerical simulations are time consuming and parameter studies quickly turn prohibitively expensive. Our work in context of the MULTIBAT project has shown that model reduction techniques such as reduced basis (RB) methods are able to vastly reduce the computational complexity of parametrized microscale battery models while retaining the full microscale features of their solutions [13, 14]. Still, such methods depend on the solution of the full high-dimensional model for selected parameters during the
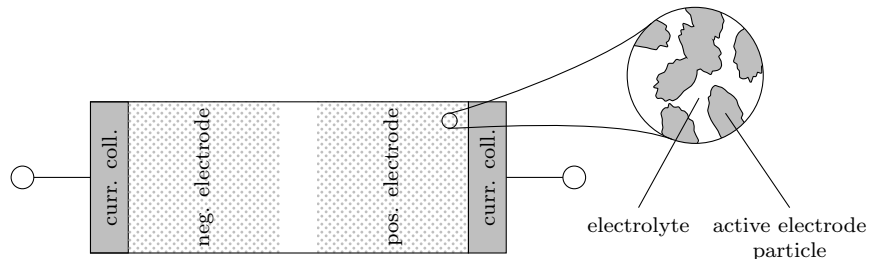
Figure 1: Sketch of a lithium-ion battery cell. The cell is connected via two metallic current collectors which are in contact with the negative/positive cell electrodes. The porous electrodes are composed of active electrode particles into which Li-ions intercalate from the electrolyte filling the pore space of the electrodes.

so-called offline phase. When only relatively few simulations of the model are required – as it is typically the case for electrochemistry simulations where one is mainly interested in the qualitative behaviour of the battery cell – the offline phase can quickly take nearly as much time as the simulation of the full model for all parameters of interest would have required. It is, therefore, paramount to reduce the number of full model solves as much possible. Localized RB methods construct spatially localized approximation spaces from few global model solves or even by only solving adequate local problems (see also [5, 6, 12] and the references therein). Thus, these methods are a natural choice for accelerating the offline phase of RB schemes, in particular for problems with a strong microscale character such as geometrically resolved electrochemistry simulations.

While localized RB methods have been studied extensively for linear problems and while there are first results for instationary problems [12, 13], we are not aware of any previous work treating nonlinear models. In this contribution, we introduce a localized RB scheme for nonlinear finite volume battery models, which builds local approximation and interpolation spaces by decomposition of global solution snapshots w.r.t. a given coarse triangulation of the computational domain (Section 5). As a preparation, we will first briefly review the microscale battery model under consideration (Section 2), its discretization (Section 3) and finally its RB approximation (Section 4). We will close with first numerical experiments that investigate the applicability of localized RB techniques to the problem at hand (Section 6).

## 2   Analytical model

As in [13, 14], we consider the microscale battery model introduced in [10] (without taking thermal effects into account and assuming constant $t_+$). In this model, the battery cell is described via coupled systems of partial differential equations for the concentration of $Li^+$-ions and the electrical potential $\phi$ for

2

each part of the cell: the electrolyte, positive and negative electrode, as well as positive and negative current collector.

In the electrolyte, the change of the concentration $c$ is governed by a diffusion process, whereas $\phi$ is determined by a stationary potential equation with source term depending non-linearly on $c$:

$$\frac{\partial c}{\partial t} - \nabla \cdot (D_e \nabla c) = 0,$$

$$-\nabla \cdot \left( \kappa \frac{1 - t_+}{F} RT \frac{1}{c} \nabla c - \kappa \nabla \phi \right) = 0.$$

In the electrodes, the evolution of $c$, i.e. the intercalation of Li-ions into the active particles, is again driven by diffusion. The potential $\phi$ no longer depends on the Li-ion distribution:

$$\frac{\partial c}{\partial t} - \nabla \cdot (D_s \nabla c) = 0,$$

$$-\nabla \cdot (\sigma \nabla \phi) = 0.$$

No Li-ions enter the metallic current collectors, so $c \equiv 0$ on this part of the domain, whereas $\phi$ is again given as:

$$-\nabla \cdot (\sigma \nabla \phi) = 0.$$

The reaction at the interface between active electrode particles and the electrolyte is governed by the so-called Butler-Volmer kinetics which determine the electric current $j = \nabla \phi \cdot n$ from the active particle into the electrolyte as

$$j = 2k \sqrt{c_e c_s (c_{max} - c_s)} \sinh \left( \frac{\phi_s - \phi_e - U_0(\frac{c_s}{c_{max}})}{2RT} \cdot F \right), \qquad (1)$$

where $c_e$, $\phi_e$ ($c_s$, $\phi_s$) are the concentration and potential on the electrolyte (solid particle) side of the interface. The Li-ion flux $N$ over the interface proportionally depends on $j$ and is given by $N = j/F$. Note that the Butler-Volmer relations ensure the coupling between both considered variables and, through the exponential dependence on the overpotential $\phi_s - \phi_e - U_0(c_s/c_{max})$, lead to a highly nonlinear behaviour of the system.

Finally, continuity conditions for $\phi$ are imposed between electrode and current collector, whereas there is no coupling between electrolyte and current collector. The following boundary conditions are imposed: $\phi = U_0(c(0)/c_{max})$ at the negative current collector boundary, Neumann boundary conditions at the positive current collector (applied fixed charge/discharge rate) and periodic boundary conditions for $c$ and $\phi$ at the remaining domain boundaries. We denote the initial concentration at time $t = 0$ by $c_0 = c(0)$, the final time is denoted as $T$. All appearing natural/material constants as well as the initial data is summarised in Table 1.

Table 1: Constants used in the battery model. The open circuit potential $U_0$ for a state of charge $s$ is give as $U_0(s) = (-0.132 + 1.41 \cdot e^{-3.52s}) \cdot V$ for the negative electrode and as $U_0(s) = [0.0677504 \cdot \tanh(-21.8502 \cdot s + 12.8268) - 0.105734 \cdot ((1.00167 - s)^{-0.379571} - 1.576) - 0.045 \cdot e^{-71.69 \cdot s^8} + 0.01 \cdot e^{-200 \cdot (s - 0.19)} + 4.06279] \cdot V$ for the positive electrode.

| symbol | unit | value | description |
|---|---|---|---|
| $D_e$ | $\frac{cm^2}{s}$ | $1.622 \cdot 10^{-6}$ | collective interdiffusion coefficient in electrolyte |
| $D_s$ | $\frac{cm^2}{s}$ | $10^{-10}$ | ion diffusion coefficient in electrodes |
| $\sigma$ | $\frac{s}{cm}$ | 10 <br> 0.38 | electronic conductivity in neg. electrode <br> electronic conductivity in pos. electrode |
| $\kappa$ | $\frac{s}{cm}$ | 0.02 | ion conductivity |
| $c_{max}$ | $\frac{mol}{cm^3}$ | $24681 \cdot 10^{-6}$ <br> $23671 \cdot 10^{-6}$ | maximum Li$^+$ concentration in neg. electrode <br> maximum Li$^+$ concentration in pos. electrode |
| $k$ | $\frac{Acm^{2.5}}{mol^{1.5}}$ | 0.002 <br> 0.2 | reaction rate at neg. electrode/electrolyte interface <br> reaction rate at pos. electrode/electrolyte interface |
| $c_0$ | $\frac{mol}{cm^3}$ | $1200 \cdot 10^{-6}$ <br> $2639 \cdot 10^{-6}$ <br> $20574 \cdot 10^{-6}$ | initial concentration in electrolyte <br> initial concentration in neg. electrode <br> initial concentration in pos. electrode |
| $t_+$ | | 0.39989 | transference number |
| $T$ | $K$ | 298 | temperature |
| $F$ | $\frac{As}{mol}$ | 96487 | Faraday constant |
| $R$ | $\frac{J}{mol\,K}$ | 8.314 | universal gas constant |

# 3  Finite volume discretization

Following [16], the continuous model is discretized using a basic cell centered finite volume scheme on a voxel grid. Each voxel is assigned a unique subdomain and the Butler-Volmer conditions are chosen as numerical flux on grid faces separating an electrolyte from an electrode voxel. We obtain a single nonlinear finite volume operator $A_\mu : V_h \oplus V_h \to V_h \oplus V_h$ for the whole computational domain, where $V_h$ denotes the space of piecewise constant grid functions and $\mu$ indicates a parameter we want to vary. In the following, we will consider the applied charge current as parameter of interest. Implicit Euler time stepping with constant time step size $\Delta t$ leads to the $N := T/\Delta t$ nonlinear equation systems

$$\begin{bmatrix} \frac{1}{\Delta t}(c_\mu^{(n+1)} - c_\mu^{(n)}) \\ 0 \end{bmatrix} + A_\mu \left( \begin{bmatrix} c_\mu^{(n+1)} \\ \phi_\mu^{(n+1)} \end{bmatrix} \right) = 0, \qquad (c_\mu^{(n)}, \phi_\mu^{(n)}) \in V_h \oplus V_h. \quad (2)$$

The equation systems are solved using a standard Newton iteration scheme.

Note that we can decompose $A_\mu$ as

$$A_\mu = A_\mu^{(aff)} + A^{(bv)} + A^{(1/c)} \tag{3}$$

where $A^{(bv)}, A^{(1/c)} : V_h \oplus V_h \to V_h \oplus V_h$ accumulate the numerical fluxes corresponding to (1) and $\kappa \frac{1-t_+}{F} RT \frac{1}{c} \nabla c$. Thus, the operator $A_\mu^{(aff)}$ collecting the remaining numerical fluxes is affine linear and the only operator in the decomposition depending on the charge rate. $A_\mu^{(aff)}$ can be further decomposed as

$$A_\mu^{aff} = A^{const} + \mu \cdot A^{bnd} + A^{lin}, \tag{4}$$

with constant, non-parametric operators $A^{const}, A^{bnd}$ corresponding to the boundary conditions and a non-parametric linear operator $A^{(lin)}$.

# 4 Reduced basis approximation

As reduced model we consider the Galerkin projection of (2) onto an appropriate reduced basis space $\tilde{V} \subseteq V_h \oplus V_h$, i.e. we solve

$$P_{\tilde{V}} \left\{ \begin{bmatrix} \frac{1}{\Delta t}(\tilde{c}_\mu^{(n+1)} - \tilde{c}_\mu^{(n)}) \\ 0 \end{bmatrix} + A_\mu \left( \begin{bmatrix} \tilde{c}_\mu^{(n+1)} \\ \tilde{\phi}_\mu^{(n+1)} \end{bmatrix} \right) \right\} = 0, \quad (\tilde{c}_\mu^{(n)}, \tilde{\phi}_\mu^{(n)}) \in \tilde{V}, \tag{5}$$

where $P_{\tilde{V}}$ denotes the orthogonal projection onto $\tilde{V}$. In order to obtain at an online efficient scheme, the projected operator $P_{\tilde{V}} \circ A_\mu$ has to be approximated by an efficiently computable approximation. Considering the decompositions (3) and (4), only the nonlinear operators $A_\mu^{(bv)}, A_\mu^{(1/c)}$ require special treatment for which we employ empirical operator interpolation [8] based on the empirical interpolation method [2]. Denoting the discrete time differential operator by $B$, the fully reduced scheme is then given as

$$\begin{aligned}
\Big\{ &P_{\tilde{V}} \circ B + P_{\tilde{V}} \circ A^{(const)} + \mu \cdot P_{\tilde{V}} \circ A^{(bnd)} + P_{\tilde{V}} \circ A^{(lin)} \\
&+ \{P_{\tilde{V}} \circ I_{M^{(1/c)}}^{(1/c)}\} \circ \tilde{A}_{M^{(1/c)}}^{(1/c)} \circ R_{M'^{(1/c)}}^{(1/c)} \\
&+ \{P_{\tilde{V}} \circ I_{M^{(bv)}}^{(bv)}\} \circ \tilde{A}_{M^{(bv)}}^{(bv)} \circ R_{M'^{(bv)}}^{(bv)} \quad \Big\} \left( \begin{bmatrix} \tilde{c}_\mu^{(t+1)} \\ \tilde{\phi}_\mu^{(t+1)} \end{bmatrix} \right) = 0,
\end{aligned} \tag{6}$$

where $\tilde{A}_{M^{(*)}}^{(*)} : \mathbb{R}^{M'^{(*)}} \to \mathbb{R}^{M^{(*)}}$ ($* = bv, 1/c$) denotes the restriction of $A^{(*)}$ to certain $M^{(*)}$ image degrees of freedom given the required $M'^{(*)}$ source degrees of freedom, $R_{M'^{(*)}}^{(*)} : V_h \oplus V_h \to \mathbb{R}^{M'^{(*)}}$ is the linear operator restricting finite volume functions to these $M'^{(*)}$ source degrees of freedom, and $I_{M^{(*)}}^{(*)} : \mathbb{R}^{M^{(*)}} \to V_h \oplus V_h$ is the linear interpolation operator to the $M^{(*)}$ evaluation points and an appropriately selected interpolation basis. Note that for the considered finite volume scheme we have $M'^{(*)} \leq 14 \cdot M^{(*)}$, thus $\tilde{A}_{M^{(*)}}^{(*)}$ can be computed quickly
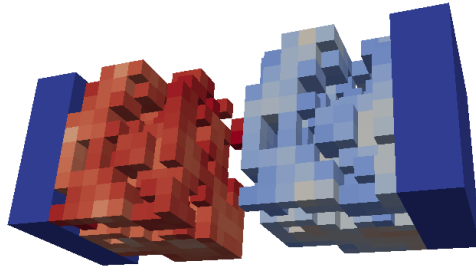
5

Figure 2: Small battery geometry used in numerical experiment. Domain: $104\mu m \times 40\mu m \times 40\mu m$, 4.600 degrees of freedom. Coloring: Li$^+$-concentration at final simulation time $T = 2000s$, electrolyte not depicted.

for sufficiently small $M^{(*)}$. The remaining terms in (6) are linear (or constant) and can be pre-computed for a given reduced basis of $\tilde{V}$.

In [13] we have considered the solution of (6) where $\tilde{V}$ and the interpolation data for $A^{(bv)}$, $A^{(1/c)}$ have been generated using standard model order reduction techniques. The reduced space $\tilde{V}$ was determined by computing a proper orthogonal decomposition (POD) [17] of solution trajectories of (2) for an equidistant training set of charge rate parameters. Since the $c$ and $\phi$ variables are defined on different scales, the POD had to be applied separately for both variables, yielding a reduced space of the form $\tilde{V} = \tilde{V}_c \oplus \tilde{V}_\phi$, in order to obtain a stable scheme. Moreover, the intermediate stages of the Newton algorithms used for solving (2) were included in the snapshot data to ensure the convergence of the Newton algorithms when solving the reduced scheme.

The interpolation bases and interpolation points have been obtained by evaluating $A^{(*)}$ on the computed solution trajectories and then performing the EI-GREEDY algorithm [7] on these evaluations. Note that for solution trajectories of (2), $A_\mu$ vanishes identically in the $\phi$-component. Thus, applying the EI-GREEDY algorithm directly to evaluations of $A_\mu$ would not have yielded usable interpolation spaces.

## 5 Localized basis generation

Localized RB methods can be seen as RB schemes where the reduced space $\tilde{V}$ has a certain direct sum decomposition $\tilde{V} = \tilde{V}_1 \oplus \ldots \oplus \tilde{V}_K$ with subspaces $\tilde{V}_i$ associated to some partition $\overline{\Omega} = \overline{\Omega_1} \cup \ldots \cup \overline{\Omega_K}$ of the computational domain $\Omega$. Since this imposes an additional constraint on the possible choices of reduced spaces $\tilde{V}$, it is not to be expected that such methods yield better approximation spaces for the same (total) dimension of $\tilde{V}$ than classical RB methods. However, these methods can yield enormous saving in computation time during basis generation. In particular, we are interested in the following aspects:

1. When the parametrization of the problem mainly affects the global so-

lution behaviour, only few global solution snapshots may be required to observe all relevant local behaviour. This can be exploited by computing local approximation spaces from global solutions which have been decomposed according to the partition $\Omega_1 \cup \ldots \cup \Omega_K$ (e.g. [1]).

2. The local approximation spaces $\tilde{V}_i$ may be enriched by solving appropriate local problems on a neighbourhood of $\Omega_i$. The solution of the local problems can be trivially parallelized, and each local problem will be solvable much faster than the global problem, which might even be unsolvable with the available computational resources (e.g. [15]).

3. When the problem undergoes local changes (e.g. geometry change due to Li-plating), the spaces $\tilde{V}_i$ which are unaffected by the change can be reused and only few new local problems have to be solved (e.g. [5]).

For many applications, the time for basis generation must be taken into account when considering the overall efficiency of the reduction scheme. Hence, such localization approaches can be an essential tool for making model order reduction profitable for these applications. This is also the case for battery simulations, where typically only relatively few parameter samples are required to gain an appropriate idea of the behaviour of the model and these same computational resources are available for all required simulations. Also note that while reduced system matrices/Jacobians are dense matrices for standard RB approaches, one typically obtains block sparse matrices for localized RB approaches, so the increased global system dimension can be largely compensated by appropriate choices of linear solvers.

In this contribution we investigate if spatially resolved electrochemistry simulations are in principle amenable to such localization techniques. For this we partition the computational domain with a cuboid macro grid with elements $\Omega_1, \ldots \Omega_K$ that are aligned with the microscale voxel grid of the given finite volume discretization (cf. Fig. 4). This partition induces a direct sum decomposition of $V_h$:

$$V_h = V_{h,1} \oplus \ldots \oplus V_{h,K}, \qquad V_{h_i} = \{f \in V_h \mid \operatorname{supp}(f) \subseteq \overline{\Omega_i}\}.$$

We now compute local reduced spaces $\tilde{V}_{c,i}$, $\tilde{V}_{\phi,i}$ by first computing global solution snapshots $c_{\mu_s}^{(n)}$, $\phi_{\mu_s}^{(n)}$ for preselected parameters $\mu_1, \ldots, \mu_S$ and then performing local PODs of the $L^2$-orthogonal projections of these snapshots onto the local finite volume spaces $V_{h,i}$. Hence,

$$\tilde{V}_{c,i} \subseteq \operatorname{span}\{P_{V_{h,i}}(c_{\mu_s}^{(n)}) \mid 1 \leq s \leq S, \ 1 \leq n \leq N\},$$
$$\tilde{V}_{\phi,i} \subseteq \operatorname{span}\{P_{V_{h,i}}(\phi_{\mu_s}^{(n)}) \mid 1 \leq s \leq S, \ 1 \leq n \leq N\}.$$

Since our high-dimensional model is already given as a non-conforming discretization, we con now simply obtain a reduced model by solving (5) with the reduced space

$$\tilde{V} = (\tilde{V}_{c,1} \oplus \ldots \oplus \tilde{V}_{c,K}) \oplus (\tilde{V}_{\phi,1} \oplus \ldots \oplus \tilde{V}_{\phi,K}).$$

7

In order to obtain a fully localized model, localized treatment of the nonlinearities $A^{(bv)}$, $A^{(1/c)}$ is required as well. Not only will most of the speedup during the offline phase be lost when the interpolation data is computed without localization. Global interpolation basis vectors will also induce a coupling between all local approximation spaces $\hat{V}_{c,i}$, $\hat{V}_{\phi,i}$. Thus the block sparsity structure of the Jacobians appearing in the Newton update problems for solving (6) is lost, strongly deteriorating reduced solution times. Moreover, the additional reduced degrees of freedom due to localization can exhibit a destabilizing effect when not accounted for while generating the interpolation spaces: in the limit when each subdomain $\Omega_i$ corresponds to a single voxel, we have $\tilde{V} = V_h \oplus V_h$ whereas the images of the interpolated operators are only $M^{(bv)}/M^{(1/c)}$-dimensional with $M^{(bv)}/M^{(1/c)} \ll \dim(V_h \oplus V_h)$.

As a first approach to localized treatment of the nonlinear operators, we proceed similar to the reduced basis generation. We first construct local empirically interpolated operators $I^{(*)}_{i,M_i^{(*)}} \circ \tilde{A}^{(*)}_{i,M_i^{(*)}} \circ R^{(*)}_{i,M_i'^{(*)}}$ ($* = bv, 1/c$) by applying the EI-GREEDY algorithm to the projected evaluations

$$\{P_{V_{h,i}}(A^{(*)}([c^{(n)}_{\mu_s}, \phi^{(n)}_{\mu_s}]^T)) \mid 1 \leq s \leq S,\ 1 \leq n \leq N\}.$$

We then obtain the localized interpolated operators

$$A^{(*)} \approx I^{(*)} \circ \tilde{A}^{(*)} \circ R^{(*)},$$

where

$$I^{(*)} = \left[ I^{(*)}_{1,M_1^{(*)}}, \ldots, I^{(*)}_{K,M_K^{(*)}} \right], \quad \tilde{A}^{(*)} = \mathrm{diag}\left( \tilde{A}^{(*)}_{1,M_1^{(*)}}, \ldots, \tilde{A}^{(*)}_{K,M_K^{(*)}} \right), \quad (7)$$

$$R^{(*)} = \left[ R^{(*)}_{1,M_1'^{(*)}}, \ldots, R^{(*)}_{K,M_K'^{(*)}} \right]^T. \quad (8)$$

Using these operators in (6) leads to a basic, fully localized and fully reduced approximation scheme for (2).

In order to obtain a stable reduced scheme, accurate approximation of the Butler-Volmer fluxes is crucial. However, each localized interpolated operator only takes interface fluxes into its associated domain $\Omega_i$ into account: Let $T_1$ be a finite volume cell at the boundary of $\Omega_i$ and $T_2$ an adjacent cell in a different subdomain $\Omega_j$, $i \neq j$. Unless both cells are selected as interpolation points for the respective operators, local mass conservation will be violated at the $T_1/T_2$ interface due to the errors introduced by empirical interpolation.

To investigate whether these jumps in the interface fluxes of the interpolated operators have a destabilizing effect, we consider the following modified scheme: We denote by $A_i'^{(*)} : V_h \oplus V_h \to V_h \oplus V_h$, ($* = bv, 1/c$) the operator which accumulates all numerical fluxes associated with $A^{(*)}$ which correspond to grid faces contained in $\overline{\Omega_i}$. Fluxes corresponding to faces which are also contained in some $\overline{\Omega_j}$, $i \neq j$, are scaled by $1/2$. This scaling ensures that we have
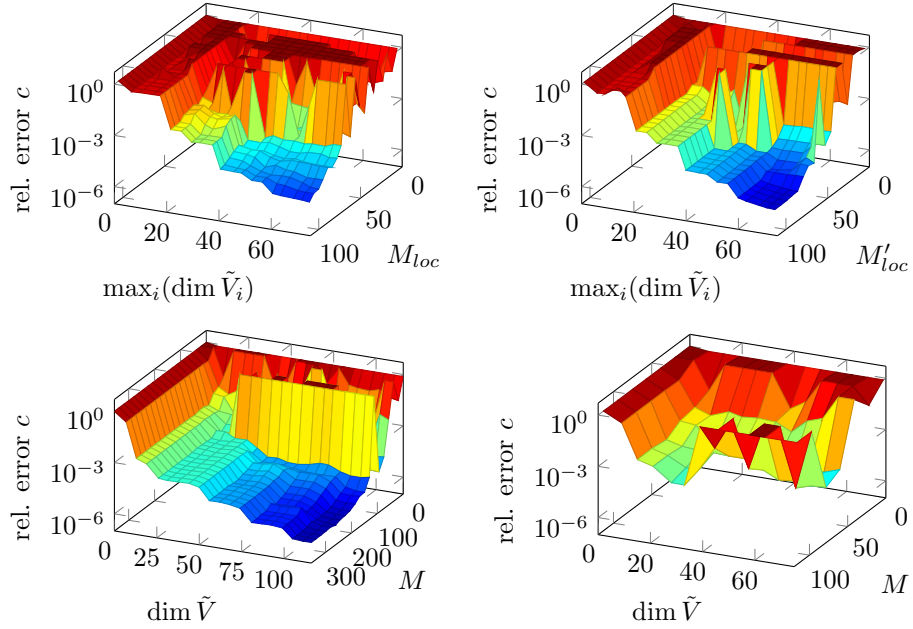
$$A^{(*)} = \sum_{i=1}^K A_i'^{(*)}.$$

Figure 3: Relative model order reduction errors for the concentration variable $c$. The error is measured in the $L^2$-in space, $L^\infty$-in time, $L^\infty$-in $\mu$ norm for 10 randomly sampled parameters $\mu \in \mathcal{P} := [0.00012, 0.0012]\,A/cm^2 \approx [0.1, 1]\,C$. Top left: errors for the fully localized scheme, $\tilde{V}_i := \tilde{V}_{c,i} \oplus \tilde{V}_{\phi,i}$, $M_{loc} := \max_i(\max(M_i^{(bv)}, M_i^{(1/c)}))$. Top right: errors for the fully localized scheme with additional special treatment of the interface fluxes, $M'_{loc} := \max_i(\max(M_i'^{(bv)}, M_i'^{(1/c)}))$. Bottom left: errors for reduced basis approximation without localization, $M := \max(M^{(bv)}, M^{(1/c)})$. Bottom right: errors for reduced basis approximation without localization with same axis scaling as in top row.

Each operator $A_i'^{(*)}$ is interpolated separately yielding approximations $I_{i,M_i^{(*)}}'^{(*)} \circ \tilde{A}_{i,M_i^{(*)}}'^{(*)} \circ R_{i,M_i'^{(*)}}'^{(*)}$, where the interpolation data is again obtained via EI-GREEDY algorithms for the evaluations

$$\left\{ A'^{(*)}([c_{\mu_s}^{(n)}, \phi_{\mu_s}^{(n)}]^T) \mid 1 \le s \le S,\ 1 \le n \le N \right\}.$$

We then proceed as before by defining $I'^{(*)}$, $\tilde{A}'^{(*)}$, $R'^{(*)}$ as in (7) and (8), obtaining the localized approximation $A^{(*)} \approx I'^{(*)} \circ \tilde{A}'^{(*)} \circ R'^{(*)}$.
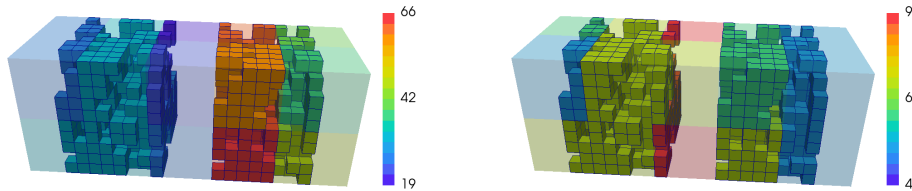
9

Figure 4: Maximum local reduced basis dimensions $\dim(\tilde{V}_{c,i})$ (left) and $\dim(\tilde{V}_{\phi,i})$ (right) obtained in the numerical experiment.

# 6 Numerical experiment

As a first numerical experiment we consider the small battery geometry depicted in Fig. 2. For this geometry we compare the performance of the two localized RB approximation schemes introduced in Section 5 with the scheme without localization described in Section 4.

The model was simulated for 2000 seconds with equidistant time steps of size $\Delta t := 10s$. In order to preclude any effects from possibly insufficient sampling of the solution manifold, the reduced models were constructed using the relatively large amount of $S = 20$ equidistant parameters in the parameter domain $\mathcal{P} := [0.00012, 0.0012] \, A/cm^2 \approx [0.1, 1] \, C$. All reduced approximation and interpolation spaces were computed with relative POD/EI-GREEDY error tolerances of $10^{-7}$. The resulting local reduced basis dimensions for the concentration and potential variables are depicted in Fig. 4. The maximum model reduction errors were estimated by computing the reduction errors for a test set of 10 random parameters and are shown for the concentration variable in Fig. 3 (the errors in the potential variable show similar behaviour). All simulations of the high-dimensional finite volume battery model have been performed within the DUNE software framework [3, 4], which has been integrated with our model order reduction library pyMOR [11].

We observe (Fig. 3, top row) that both localized schemes yield stable reduced order models with good error decay, provided a sufficiently large number of interpolation points is chosen. The localized scheme with special treatment of the boundary fluxes (top right) is indeed overall more stable than the localized scheme without boundary treatment (top left) and yields slightly smaller reduction errors.

In comparison to the global RB approximation (bottom left), less reduced basis vectors/interpolation points are required per subdomain to obtain a good approximation for the localized schemes. As expected for localized RB schemes, the total number of basis vectors/interpolation points is larger (cf. bottom right) than for the global scheme, however. Given the small size of the full order model, we cannot expect any speedup for the localized reduced models. Nevertheless, based on our experience with global RB approximation of this model [13], we expect only a small increase in the number of required basis vectors/interpolation

points to approximate larger, finely resolved geometries. Thus, good speedups can be expected for large-scale applications. Verifying this hypothesis, as well as developing algorithms for efficient localized construction and enrichment of the local approximation spaces, will be subject to future work.

# 7 Conclusion

In this contribution we demonstrated the applicability of the Localized Reduced Basis Method for an instationary nonlinear finite volume Li-ion battery model with resolved pore scale electrode geometry. To this end, we have extended the Localized Reduced Basis Method to parabolic systems of equations, while simultaneously employing the localized empirical operator interpolation in order to deal with the strong nonlinearities of the underlying electrochemical reaction processes. Numerical experiments were given to demonstrate the model order reduction potential of this approach.

# References

[1] Albrecht, F., Haasdonk, B., Ohlberger, M., Kaulmann, S.: The localized reduced basis multiscale method. Proceedings of Algoritmy 2012, Conference on Scientific Computing, Vysoke Tatry, Podbanske, September 9-14, 2012 pp. 393–403 (2012)

[2] Barrault, M., Maday, Y., Nguyen, N.C., Patera, A.T.: An 'empirical interpolation' method: application to efficient reduced-basis discretization of partial differential equations. C. R. Math. Acad. Sci. Paris **339**(9), 667–672 (2004)

[3] Bastian, P., Blatt, M., Dedner, A., Engwer, C., Klöfkorn, R., Kornhuber, R., Ohlberger, M., Sander, O.: A generic grid interface for parallel and adaptive scientific computing. II. Implementation and tests in DUNE. Computing **82**(2-3), 121–138 (2008)

[4] Bastian, P., Blatt, M., Dedner, A., Engwer, C., Klöfkorn, R., Ohlberger, M., Sander, O.: A generic grid interface for parallel and adaptive scientific computing. I. Abstract framework. Computing **82**(2-3), 103–119 (2008)

[5] Buhr, A., Engwer, C., Ohlberger, M., Rave, S.: Application of the ArbiLoMod to problems of electrodynamics. In: Proceedings of MoRePaS III (2015)

[6] Buhr, A., Engwer, C., Ohlberger, M., Rave, S.: ArbiLoMod, a simulation technique designed for arbitrary local modifications. arXiv e-prints (1512.07840) (2015). Http://arxiv.org/abs/1512.07840 (submited to SISC)

[7] Drohmann, M., Haasdonk, B., Ohlberger, M.: Reduced basis approximation for nonlinear parametrized evolution equations based on empirical operator interpolation. SIAM J. Sci. Comput. **34**(2), A937–A969 (2012)

[8] Haasdonk, B., Ohlberger, M., Rozza, G.: A reduced basis method for evolution schemes with parameter-dependent explicit operators. Electron. Trans. Numer. Anal. **32**, 145–161 (2008)

[9] Hein, S., Latz, A.: Influence of local lithium metal deposition in 3d microstructures on local and global behavior of lithium-ion batteries. Electrochimica Acta **201**, 354 – 365 (2016)

[10] Latz, A., Zausch, J.: Thermodynamic consistent transport theory of li-ion batteries. Journal of Power Sources **196**(6), 3296 – 3302 (2011)

[11] Milk, R., Rave, S., Schindler, F.: pyMOR - generic algorithms and interfaces for model order reduction. Accepted for publication in SIAM J. Sci. Comput. (2016)

[12] Ohlberger, M., Rave, S., Schindler, F.: True error control for the localized reduced basis method for parabolic problems. In: Proceedings of MoRePaS III (2015)

[13] Ohlberger, M., Rave, S., Schindler, F.: Model reduction for multiscale lithium-ion battery simulation. In: Numerical Mathematics and Advanced Applications - ENUMATH 2015 (to appear), LNCSE. Springer (2016). DOI 10.1007/978-3-319-39929-4

[14] Ohlberger, M., Rave, S., Schmidt, S., Zhang, S.: A model reduction framework for efficient simulation of li-ion batteries. In: J. Fuhrmann, M. Ohlberger, C. Rohde (eds.) Finite Volumes for Complex Applications VII-Elliptic, Parabolic and Hyperbolic Problems, *Springer Proceedings in Mathematics & Statistics*, vol. 78, pp. 695–702. Springer International Publishing (2014)

[15] Ohlberger, M., Schindler, F.: Error control for the localized reduced basis multiscale method with adaptive on-line enrichment. SIAM J. Sci. Comput. **37**(6), A2865–A2895 (2015)

[16] Popov, P., Vutov, Y., Margenov, S., Iliev, O.: Finite volume discretization of equations describing nonlinear diffusion in li-ion batteries. In: I. Dimov, S. Dimova, N. Kolkovska (eds.) Numerical Methods and Applications, *Lecture Notes in Computer Science*, vol. 6046, pp. 338–346. Springer Berlin Heidelberg (2011)

[17] Sirovich, L.: Turbulence and the dynamics of coherent structures. i-coherent structures. ii-symmetries and transformations. iii-dynamics and scaling. Quarterly of Applied Mathematics **45**(3), 561–571 (1987)